.

Generation of OAM entangled two-photon states in the Laguerre–Gauss modes basis

UNIVERSIDAD DE GUANAJUATO

CENTRO DE INVESTIGACIONES EN OPTICA, A.C.

Fátima Quijas Escalera

Advisors:

Dr. Carlos Herman Wiechers Medina and Dr. Roberto Ramírez Alarcón

Contents

"Poem for Quantum Computing Skeptics

Quantum computers may at first sight seem
To be impossible. How dare we dream
Of solving problems that else would take more time
Than has passed since the primeval Big Bang!

But is there any reason to believe
The universe computes the way we do?
Nature is profligate with galaxies.
Why shouldn't her extravagance hold true
For other things? Why mightn't she achieve
Prodigious feats of computation, too".

Peter Shor

Acknowledgments

Quisiera empezar extendiendo mi más sincera gratitud a la Universidad de Guanajuato, que ha sido parte de mi formación, y por estos 7 años ha puesto en mi camino a grandes profesores, compañeros y amigos.

Al Centro de Investigaciones en Óptica por darme la oportunidad de trabajar en lo que me fascina, en especial gracias al Dr. Carlos Wiechers, Dr. Roberto Ramírez, y Aarón, sin ellos este trabajo no sería lo que es.

Igualmente, esto ha sido posible gracias a todas esas personas que me orientaron y apoyaron a lo largo de mi carrera, Dr Rigoberto, Dr. Ignacio, Dr. James Stotz, María, Dani, y Hala.

Finalmente quisiera destacar que este trabajo es el resultado de un sinfín de acontecimientos que poco tuvieron que ver con lo académico, sino más bien, con el amor y la amistad. Gracias a mi familia, en especial a mi mamá, Mónica y mi papá, Víctor, por su esfuerzo y apoyo día a día, y a mis hermanos, cada uno apoyándome a su manera. A mis amigos Leslie, Joss, Lilian, Vale, y Dani. Gracias por estar conmigo en este proceso.

Nada de esto hubiera sido posible sin ustedes.

Introduction

Entangled photonic quantum states play a vital role in revolutionary quantum information and quantum computation technologies [1, 2, 3]. Entangled states of higher-dimensional systems offer an increase in the information capacity per photon; a highly desirable property. However, it is challenging to experimentally implement such states.

Particle entanglement, firstly introduced as an objection in the Einstein, Podolsky, and Rosen (EPR) thought experiment, is one of the most fascinating elements of quantum mechanics. Entanglement represents the notion of non-local quantum correlations between two or more quantum-mechanical systems in the sense that the action of measuring an observable for one of a pair of entangled particles, immediately determines the corresponding value for the other particle, regardless of their separation. This property disturbed many scientists and resulted in the emergence of hidden variable theories, which propose that nature operates through local processes with unknown (hidden) variables determining observables.

Bell's inequality and its extension, Clauser-Horne-Shimony-Holt (CHSH) Bell's inequality, enabled practical experiments to test quantum theory against local hidden variable theories. Multiple experiments violated Bell's inequality, confirming quantum mechanical predictions of entanglement. In 2001, it was discovered that orbital angular momentum (OAM) could also serve as a degree of freedom for generating entangled photonic quantum states, offering advantages in terms of dimensionality [4].

In this work, it is presented a theoretical description and the corresponding experimental implementation of OAM entangled two-photon quantum state, decomposed in terms of the Laguerre-Gauss modes basis (LG). The photon pairs are produced through a type-I Spontaneous Parametric Down-Conversion (SPDC) process in a collinear configuration and manipulated using computer-controlled holograms. The experimental characterization of the OAM entangled states consisted on measuring the OAM correlations of the photon pairs produced by SPDC, in order to reconstruct the Spiral Bandwidth (SBW) of the two-photon state. Then, we proceed to certify the entanglement of the state by measuring the violation of Bell-type inequalities.

It is important to mention that this work represents a preliminary stage of a long term project of the Quantum Photonics Laboratory at CIO, aimed to implement free space quantum communication systems exploiting OAM entangled two photon states in different modal basis, such as Laguerre-Gauss or Ince-Gauss.

1 Paraxial Wave Equation

Starting from the basics, the families of solutions to the paraxial wave equation, such as Hermite-Gauss, Laguerre-Gauss, Bessel-Gauss, and Ince-Gauss beams, among others, are of great importance in explaining the correlation in OAM between the photon pairs from the SPDC process. Each of these beams represents a set of light modes with unique spatial distribution and phase profile properties, which allow them to carry intrinsic orbital angular momentum (OAM), which will be explained in more detail in the section 2.

In order to describe the propagation of light in free space, we start by considering Maxwell's equations:

$$\vec{\nabla} \cdot \mathbf{E} = 0, \tag{1.1a}$$

$$\vec{\nabla} \cdot \mathbf{B} = 0, \tag{1.1b}$$

$$\vec{\nabla} \times \mathbf{E} = -\frac{\partial}{\partial t}\mathbf{B}, \tag{1.1c}$$

$$\vec{\nabla} \times \mathbf{B} = \frac{1}{c^2}\frac{\partial}{\partial t}\mathbf{E}. \tag{1.1d}$$

By decoupling the Faraday's Law we can obtain the wave equation for the $\mathbf{E}$-field [5].

$$\nabla^2\mathbf{E} - \frac{1}{c^2}\frac{\partial^2}{\partial t^2}\mathbf{E} = 0, \tag{1.2}$$

similarly for the field $\mathbf{B}$:

$$\nabla^2\mathbf{B} - \frac{1}{c^2}\frac{\partial^2}{\partial t^2}\mathbf{B} = 0 \tag{1.3}$$

Plane waves are impossible to generate since they carry an infinite amount of energy [5]. To construct a paraxial wave can be started with a plane wave Ae^{-jkz}. In order that the complex amplitude of the field $U(\mathbf{r}) = A(\mathbf{r})e^{-jkz}$ satisfy the Helmholtz equation, $\nabla^2 U + k^2 U = 0$. By making the substitution with $A(\mathbf{r})$, the Helmholtz equation becomes [6]

$$\left(\frac{\partial^2}{\partial x^2} + \frac{\partial^2}{\partial y^2}\right) A + \frac{\partial^2}{\partial z^2}A + 2\mathrm{j}k\frac{\partial}{\partial z}A = 0.$$

If variation of the amplitude u in the z direction is slow, so is possible to do a paraxial approximation [7]:

$$\nabla_T^2 A - j2k\frac{\partial A}{\partial z} = 0, \tag{1.4}$$

where $\nabla_T^2 = \partial^2/\partial x^2 + \partial^2/\partial y^2$ is the transverse Laplacian operator [6]. That is equivalent to the Schrödinger equation in two dimensions [7].

1.1 Families of Solutions of the Paraxial Helmholtz Equation

1.1.1 Gaussian Beam

A simple solution to the paraxial Helmholtz equation yields the paraboloidal wave, which is the paraxial approximation of the spherical wave.

One of the most interesting and useful solutions is the Gaussian beam, which complex envelope is [6]:

$$A(\mathbf{r}) = \frac{A_1}{q(z)} \exp\left[-jk\frac{\rho^2}{2q(z)}\right], \quad q(z) = z + jz_0. \tag{1.5}$$

The q-parameter, $q(z)$ defines the peak amplitude and beam axis. The distance to the beam waist z and the Rayleigh range z_0. Write the complex function $1/q(z)$ in terms of its real and imaginary parts by defining two new real functions that are measures of the beam width, $W(z)$, and the wavefront radius of curvature, $R(z)$. With this, we can obtain the expression of the complex amplitude $U(\mathbf{r})$ of the Gaussian beam [6]:

$$U(\mathbf{r}) = A_0 \frac{W_0}{W(z)} \exp\left[-\frac{\rho^2}{W^2(z)}\right] \exp\left[-jkz - jk\frac{\rho^2}{2R(z)} + j\zeta(z)\right] \tag{1.6}$$

The parameters required to characterize a Gaussian beam are its peak amplitude, determinate by A_0, its direction (the beam axis), the location of its waist, and the waist radius W_0 or the Rayleigh range z_0 [6].

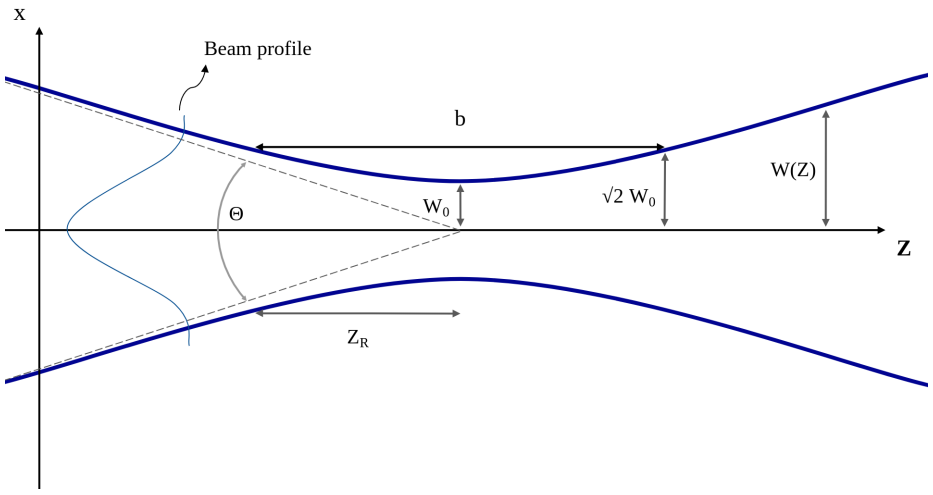

Figure 1.1: Schematic imagine of the Gaussian beam. WhereW_0 is the beam waist, the Rayleigh length Z_R and the beam divergence θ.

A Gaussian beam acquires a phase shift along its direction of propagation that is different from that of a plane wave with the same optical frequency. The Gouy phase shift is the name given to this variation. $\zeta(z)$ [6]. The Gouy phase describes how the phase distribution of the wave changes as it propagates outward from the waist of the beam. As the wave moves away from the waist of the beam, the Gouy phase changes slowly, reaching its maximum value $(\pi/2)$ in a plane perpendicular to the direction of propagation in what is known as the "plane of Gouy". After passing through the Gouy plane, the phase begins to decrease again as the wave continues to propagate.

1.1.2 Laguerre-Gaussian beam

Expressing the paraxial Helmholtz equation in cylindrical coordinates (ρ, ϕ, z) and employing the separation-of-variables method in ρ and ϕ instead of x and y allows the representation of the complex amplitude of the Laguerre-Gaussian beam, denoted as LG_{lm}, as[6]:

$$\begin{aligned} U_{l,m}(\rho,\phi,z) = A_{l,m}\left[\frac{W_0}{W(z)}\right]\left(\frac{\rho}{W(z)}\right)^l \mathbb{L}_m^l\left(\frac{2\rho^2}{W^2(z)}\right)\exp\left(-\frac{\rho^2}{W^2(z)}\right) \\ \times \exp\left[-jkz - jk\frac{\rho^2}{2R(z)} \mp jl\phi + j(l+2m+1)\zeta(z)\right], \end{aligned} \tag{1.7}$$

where the $\mathbb{L}_m^l(\cdot)$ represent generalized Laguerre polynomials. $l = 0, 1, 2, \ldots$ is aziuthal and $m = 0, 1, 2, \ldots$ are radial indices.

The Laguerre-Gaussian beam's intensity is circularly symmetric (see fig. 1.2). Its maximum value occurs at a radius of $\rho = \sqrt{1/2}W(z)$. For beams where $l \neq 0$, intensity at the beam center $(\rho = 0)$ is zero; those with a radial index $m > 0$ manifest as multiple ring patterns [6].

The Gouy phase in the Laguerre-Gaussian beam intensifies by the factor $(l + 2m + 1)$, and an extra phase factor $e^{\pm jl\phi}$, where ϕ is the azimuthal angle. The most basic Laguerre-Gaussian beam LG_{00}, similar to the Hermite-Gaussian beam HG_{00}, corresponds to a Gaussian beam [4, 8].

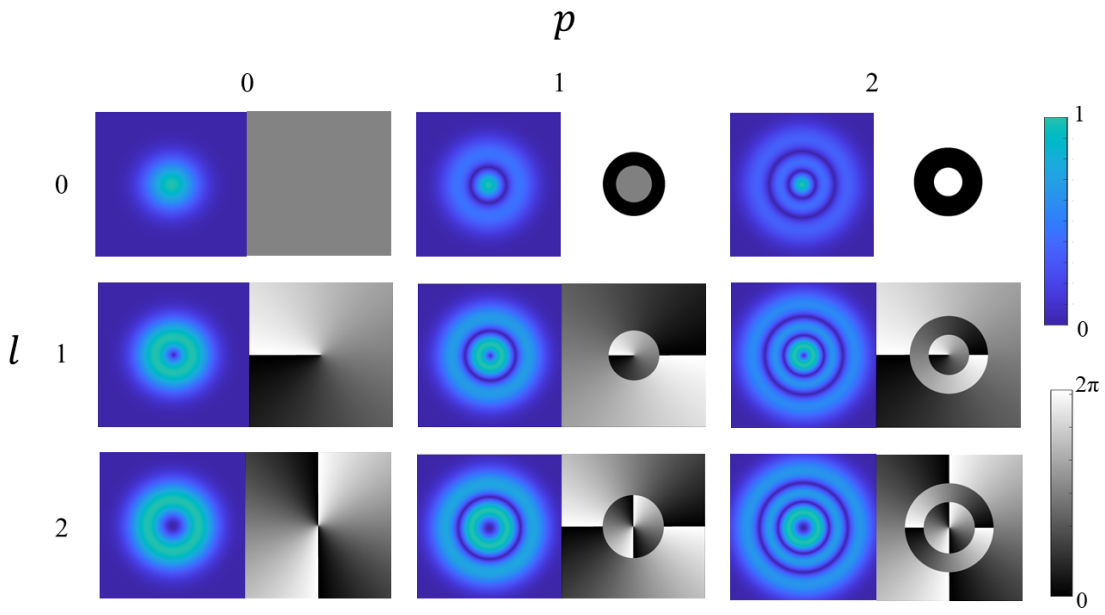

Figure 1.2: Laguerre-Gaussian beams intensity distributions (left) and phase (right).

2 Angular Momentum of light

2.1 Angular Momentum

The way photons interact with different components and change their properties, for example, polarizers, makes them ideal for studying entanglement. Photons are fundamental information carriers. They have many degrees of freedom in which they can transmit information, including: phase, energy, linear momentum, and polarization. In recent years, another has been discovered: their orbital angular momentum (OAM)[9].

The light has two contributions to its angular momentum [8]; one that is related to the polarization of the field, known as Spin Angular Momentum (SAM), and the part that is determined by the azimuthal phase dependence, which is known as Orbital Angular Momentum (OAM). In this section, both types are described. With a focus on the description of their relationship with helical beams, such as the Laguerre-Gaussian beams described in section 1, as well as the process of detecting and generating beams carrying OAM [10].

2.1.1 Spin Angular Momentum

Spin is often considered a property of massive particles. However, this characteristic can also be attributed to photons, even if they are massless [11].

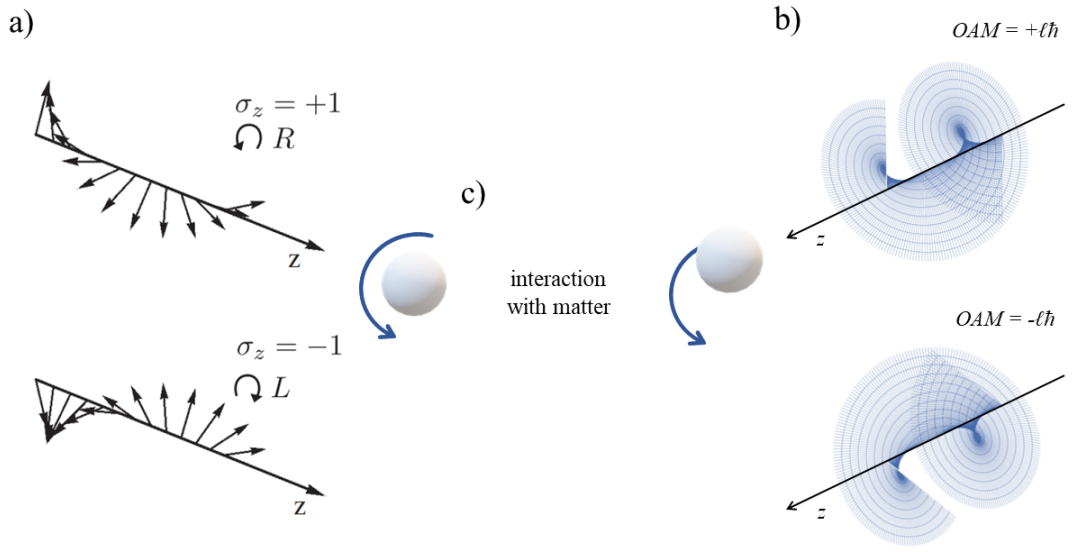

Figure 2.1: a) Spin angular momentum (SAM) ($\sigma_z\hbar$). Counterclockwise rotation (R) polarisation with $\sigma_z = 1$ and clockwise, polarisation $\sigma_z = -1$. b) Orbital angular momentum (OAM) can also be counterclockwise $+\ell\hbar$ or clockwise $-\ell\hbar$. c) Interaction angular momentum of light with matter. SAM, in a light beam with circular polarization, makes an object rotate around its axis. OAM, from a light beam with phase distribution, makes the object rotate about the central axis of the beam.

Spin Angular momentum is the result of the circulating flow of energy in an electromagnetic field, arises from the rotation of the light electric field during beam propagation [11, 8] (figure 2.1 (a)).

The SAM, per photon, has a value of $\sigma_z\hbar$, where σ_z is determined by the polarization.

The polarization state can be represented as a superposition of right and left circular polarizations $\sigma_z = 0$ [9, 8].

2.1.2 Orbital Angular Momentum

Darwin studied radiation processes and concluded that "For quadrupole emission, the pure particle concept is a failure" [12]. The emitted photon must carry not only spin but also OAM, and he proposes an expressions for each of these components [13].

An electromagnetic wave propagates with an electric and magnetic field $\vec{E}, \vec{B}$. Let us first consider the energy density associated with the wave [5]

$$u = \frac{1}{2}\left(\epsilon_0 \vec{E}^2 + \frac{1}{\mu_0}\vec{B}^2\right)$$

Where ϵ_0 is the electrical permittivity and μ_0 is the magnetic permeability of the vacuum.

The total angular momentum of the electromagnetic field is [14]

$$\mathbf{J} = \epsilon_0 \int \mathbf{r} \times (\mathbf{E} \times \mathbf{B}) d\mathbf{r}$$

It is generally expected by atomic physics [14]

$$\mathbf{J} = \mathbf{L} + \mathbf{S}$$

where $\mathbf{L}$ represents OAM and $\mathbf{S}$ the spin $\mathbf{L}$ [14, 15].

The Helmholtz equation Eq. 1.7 and its solution was obtained in the first section. The Laguerre Gaussian modes (equation 1.4) due to their azimuthal phase dependence, are of particular interest, in $e^{i\ell\phi}$. This term suggests the existence of a phase vortex at $\rho = 0$; if we follow a closed path around this axis, we accumulate phase $2\pi\ell$ [16].

2.2 Light Beams Carrying Orbital Angular Momentum

The vortex is characterized by a number called the topological charge, which indicates how many times the light rotates per wavelength. The greater the number of revolutions, the faster the light rotates around its axis. Therefore, theoretically, the OAM carried by the optical vortex has an infinite number of eigenstates and is defined in the infinite-dimensional Hilbert vector space [17].

The OAM beams are also called a type of cylindrical vortex beam because they have zero transverse intensity along the optical axis (see figure 2.2). This is due to the phase singularity, since the electric field must be continuous it is modulated to be zero at the center [18, 13].

The LG beams were first produced using a cylindrical lens[19, 16, 8] but were more easily produced using diffractive optical elements such as diffraction gratings. A grating illuminated by a Gaussian beam, the first order diffraction beam contains a phase singularity, $e^{i\ell\phi}$, that is the phase relationship of the wavefronts spiral. The helical beams are also produced using precision-fabricated spiral phase plates that cause the beam to propagate through a spiral phase front (see Figure 2.3 (a)) [19, 8]

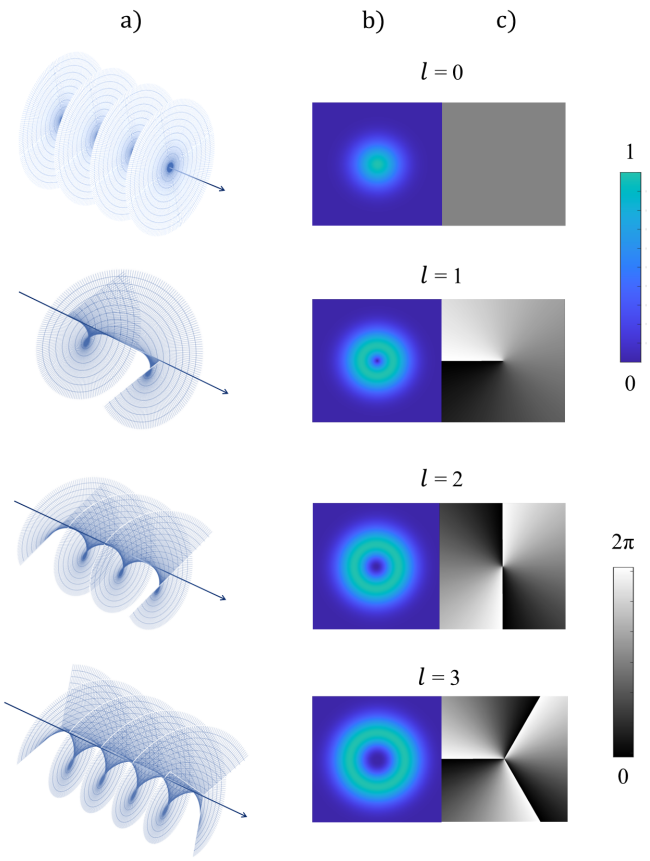

Figure 2.2: (a) Helical beam structure, the sign of the topological charge determines the direction of rotation of the wavefront.(b) Intensity amplitude of the OAM carrier beam. (c) Phase front for phase from 0 to 2π.

The OAM beams can also be generated by ℓ-forked diffraction gratings introduced by Soskin[16](fig. 2.3 (b)). On the contrary direction, if the helical phase beam interacts with the ℓ-forked hologram, it can be converted back to the fundamental Gaussian mode.This allows the processed beam to be combined into a single-mode fiber and detected by a photon detector [8], see 2.4 (b).

The most important propertie of the non-zero OAM beams, for this research project, is the orthogonality between modes. Given two OAM waves with topological charges ℓ_1 and ℓ_2, it can be seen that these two OAM modes are orthogonal through the dot product [20].

$$\int_0^{2\pi} e^{i\ell_1\theta} \left(e^{i\ell_2\theta}\right)^* d\theta = \begin{cases} 0 & \ell_1 \neq \ell_2 \\ 2\pi & \ell_1 = \ell_2 \end{cases}$$

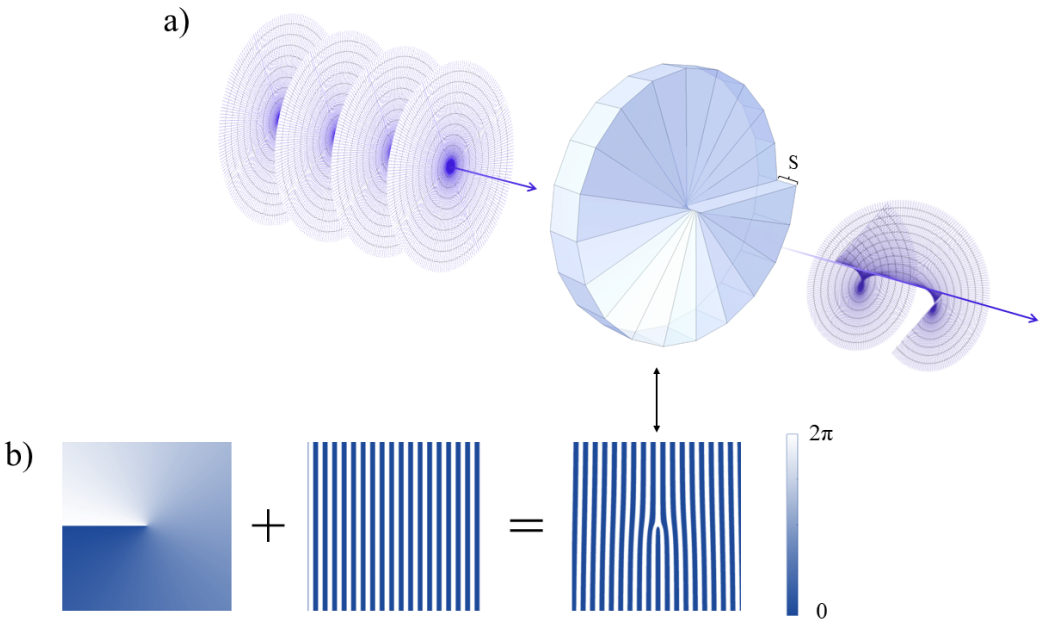

Figure 2.3: LG beam created by a (a) spiral phase plate, (b) holographically, for $\ell = 1$.

Due this property, OAM beams with different ℓ can be used as a set of separate data channels in a quantum communication systems [20].

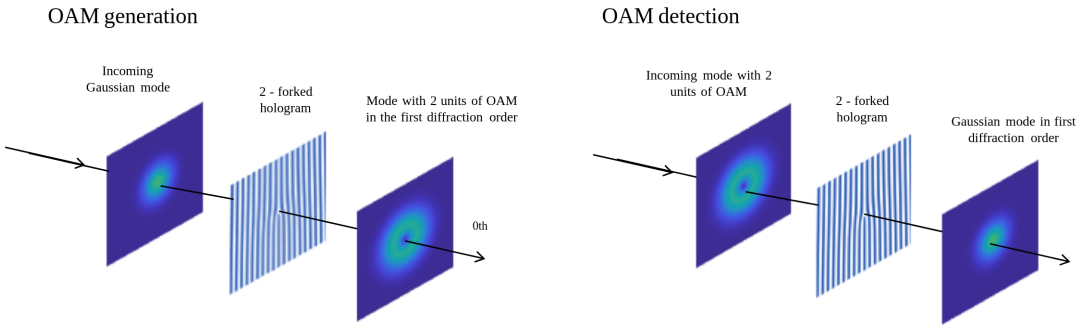

Figure 2.4: The holograms can be used to generate a beam with a helical phase front (a), and for detection, if a helical phased beam is incident on the forked diffraction grating, the beam is transformed into the fundamental Gaussian mode, so the photons of the beam can be introduced in the single mode fiber.

3 Spontaneous Parametric Down-Conversion

Introduced by Kleinman, in 1968, he defined SPDC as optical parametric noise, who also derived the interaction Hamiltonian [21]. First, some basic concepts of nonlinear optics are superficially described with a focus on the exact reverse process of SPDC, the Second Harmonic Generation (SHG) [22]. Equally superficially, the state generated in SPDC expressed in terms of the wave vector is discussed, without details of the quantization [23] as this is beyond the scope of this project.

The aim is to understand how we can express the spectrum of modes obtained from the SPDC process in the basis of special functions, such as Laguerre-Gaussian beams [24]. And how we can justify and experimentally obtain a correlation between the generated photon pairs [25].

3.1 Foundations of nonlinear optics

The induced polarization, $\tilde{\mathbf{P}} = \epsilon_0 \chi_e \tilde{\mathbf{E}}$, and magnetization, $\tilde{\mathbf{M}} = \chi_m \tilde{\mathbf{H}}$, result from the nonlinear interaction of pump radiation with a medium. Begin ϵ the permittivity, and permeability, μ, as they are related to the electric and magnetic susceptibilities of the medium, χ_e, and χ_m

It's possible to expand the nonlinear polarization into a power series to account for nonlinear dependencies on the E field in the applied radiation field, as

$$\hat{P}_i = \chi^{(1)}_{i,j} \hat{E}_j + \chi^{(2)}_{i,j,k} \hat{E}_j \hat{E}_k + \chi^{(3)}_{i,j,k,l} \hat{E}_j \hat{E}_k \hat{E}_l + \cdots$$

where $\chi^{(n)}$ is the n th-order electric susceptibility tensor [26] and where repeated indices imply a sum.

The second order non-linear polarization can be defined as [26]:

$$\tilde{\mathbf{P}}(t)^{(2)} = \epsilon_0 \chi^{(2)} \tilde{\mathbf{E}}^2(t) \tag{3.1}$$

Expressing the incident electric field as a sum of different frequencies [26, 8], different second-order nonlinear processes depend on the sign. The case $n = m$ results in Second Harmonic Generation (SHG). When $n \neq m$, that is $\omega = \pm(\omega_n \pm \omega_m)$, a Sum Frequency Generation (SFG), or Difference Frequency Generation (DFG), depending on the sign.

3.2 Classical non-linear description

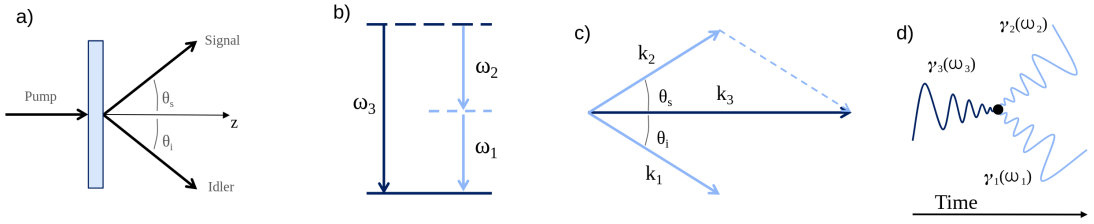

Figure 3.1: Schematic of SPDC process [24, 27, 28]. a) A pump photon of frequency ω_p spontaneously decays into two photons. b) Energy conservation. c) Momentum conservation, θ_s and θ_i are the angle of propagation of the signal and idler photons. d) SPDC Feynman's diagram.

As a parametric process, the angular frequencies photons keep energy conservation [28, 8],

$$\omega_p = \omega_s + \omega_i \tag{3.2}$$

The SPDC emission efficient when the wave vectors of the photons satisfy the conservation of linear momentum [28, 8],

$$\overrightarrow{k_p} = \overrightarrow{k_s} + \overrightarrow{k_i} \tag{3.3}$$

The last equations 3.2 and 3.3 represent the phase-matching conditions. There are different types of SPDC, including type I SPDC (superior scheme figure 3.2), in which the pump photon is $\hat{e}$ polarized and the signal and idler photons are $\hat{o}$ -polarization ($e \rightarrow oo$). In type II SPDC, the pump photon remains $\hat{e}$-polarized, but the signal and idler photons are $\hat{e}$-polarized and $\hat{o}$ -polarization ($e \rightarrow eo$) [8].

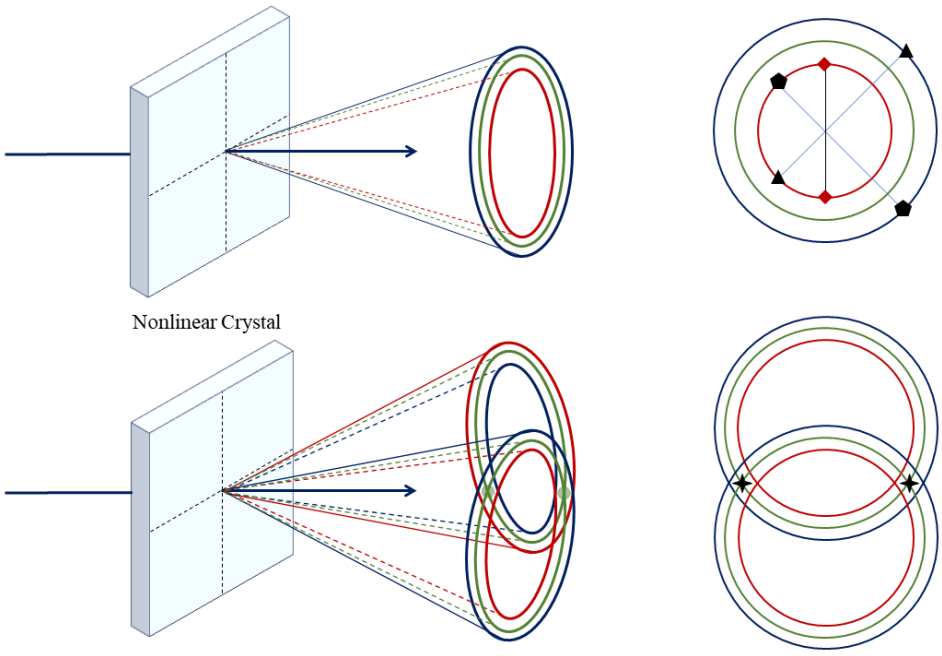

Figure 3.2: Types of Geometries in Spontaneous Parametric Down-Conversion. a) egenerate type I SPDC, b) noncollinear type II SPDC.

As a nonlinear process, a high frecuency light pump is needed, a coherent ultraviolet laser is usually used, and the pair of photons generated, are in the visible spectral range [23, 8].

3.3 Quantum description

The interaction Hamiltonian taken from [23] in the nondegenerate case, and assuming the pump field to be quantized is

$$\hat{H}_I \sim \chi^{(2)} \hat{a}_{\mathrm{p}} \hat{a}_{\mathrm{s}}^{\dagger} \hat{a}_{\mathrm{i}}^{\dagger} + H.c.$$

begin $\hat{a}_{\mathrm{p}}$ the annihilation operator of the pump beam and, $\hat{a}_{\mathrm{s}}^{\dagger}$ and $\hat{a}_{\mathrm{i}}^{\dagger}$ are the creation operators of the signal and idler photons [23].

For example case for initially in idler and signal vacuum states $|0\rangle_{\mathrm{s}}|0\rangle_{\mathrm{i}}$ [23]:

$$|1\rangle_{\mathrm{p}}|0\rangle_{\mathrm{s}}|0\rangle_{\mathrm{i}} \Rightarrow \hat{a}_{\mathrm{p}} \hat{a}_{\mathrm{s}}^{\dagger} \hat{a}_{\mathrm{i}}^{\dagger} |1\rangle_{\mathrm{p}}|0\rangle_{\mathrm{s}}|0\rangle_{\mathrm{i}} = |0\rangle_{\mathrm{p}}|1\rangle_{\mathrm{s}}|1\rangle_{\mathrm{i}}$$

Burnham and Weinberg [25] used coincidence counting observe to maintain the momentum and energy conservation and to have equal time delays of the idler and signal photons. It can be assumed that both photons are generated simultaneously.

3.4 OAM conservation

The SPDC process can have different geometries (see 3.2) if the cone angle is sufficiently closed, the resulting beam can be approximated to a paraxial beam and, distribution of modes described on bases like Laguerre-Gauss beams [24], as discussed in the first chapter. In the succeeding subsection, the theoretical justification is described. In this section, an indispensable concept for the explanation of the results obtained, the Orbital Angular Momentum conservation, is briefly introduced. It is widely accepted that in collinear type-I SPDC, OAM is conserved [29, 30, 31],

$$m = \ell_s + \ell_i \tag{3.4}$$

begin $m\hbar$ the OAM per photon of the pump beam and $\ell_i\hbar$ are the idler and $\ell_s\hbar$ signal OAM [24]. 'The probability of measuring photons in the states for the generated two-photon state. $|m-\ell\rangle$ and $|\ell\rangle$ is $|c_\ell|^{2}$' [8] can be expresed then as:

$$|\psi\rangle = \sum_{\ell=-\infty}^{+\infty} c_\ell |m-\ell\rangle|\ell\rangle \tag{3.5}$$

This correlation between the down-converted photons was first demonstrated experimentally by Zelinger et al. [32, 33] where they observe that when a nonlinear crystal is pumping by a Gaussian mode of $\ell = 0$, it is anticipated that the resulting two down-converted photons will possess opposite values of OAM, specifically $\ell_1 = -\ell_2$. To demonstrate this, the OAM of photon

A was measured after being projected onto ℓ_1, while observing the corresponding OAM of its partner photon. As anticipated, the partner photon consistently exhibits opposite values of orbital angular momentum. The previous step to the demonstration of entanglement.

3.5 Spiral bandwidth aproximation

The mode function in SPDC is the spatial and spectral shape of the created photon modes. The photon pairs generated during the SPDC process are distributed over a number of spatial modes [27].
Understanding the mode function is important in optimizing the efficiency and quality of the photon pairs generated in SPDC [24].

It is possible to decompose an electromagnetic field as a series of plane waves, as well as in other basis. A quantum state can be decomposed as a sum of LG modes, that are eigenstates of the OAM operator [14]. For the case of a single photon state:

$$|l,p\rangle = \int d\mathbf{k} LG_p^l(\mathbf{k})\hat{a}^\dagger(\mathbf{k})|0\rangle$$

The $\hat{a}^\dagger$ operator creates a photon in the plane-wave spatial mode with transverse wave-vector $\boldsymbol{q}$ [8]. And the LG_p^l modes are expresed in eq. (1.7), [27].

Using this basis, SPDC output can be expresed in the wave-vector domain [34], as

$$|\psi\rangle = \iint d\mathbf{k}_s d\mathbf{k}_i \Phi\left(\mathbf{k}_s,\mathbf{k}_i\right)\hat{a}_s^\dagger\left(\mathbf{k}_s\right)\hat{a}_i^\dagger\left(\mathbf{k}_i\right)|0\rangle \tag{3.6}$$

$\Phi\left(\mathbf{k}_s,\mathbf{k}_i\right)$ begin the mode function of the pump and the phase matching conditions [34].
If OAM is conserved, it means $l_p = l_s + l_i$. For a Gaussian pump beam, $l_p = 0$, the mode amplitude can be obtained by projecting the bi-photon SPDC state onto the target modes (eq. (3.6)) [34]:

$$\begin{aligned} C_{p_s,p_i}^{\ell_s,\ell_i} &= \langle l_s,p_s,l_i,p_i \mid \psi_{\mathrm{SPDC}}\rangle \\ &= \langle \psi_s,\psi_i \mid \psi_{\mathrm{SPDC}}\rangle \\ &= \iint d^3k_s d^3k_i \Phi\left(\mathbf{k}_s,\mathbf{k}_i\right)\left[\mathrm{LG}_{p_s}^{\ell_s}\left(\mathbf{k}_s\right)\right]^*\left[\mathrm{LG}_{p_i}^{\ell_i}\left(\mathbf{k}_i\right)\right]^* \end{aligned} \tag{3.7}$$

$P_{p_s,p_i}^{\ell_s,\ell_i} = \left|C_{p_s,p_i}^{\ell_s,\ell_i}\right|^2$ is he coincidence probability of finding a photon pair LG mode (3.7).
The integration limits depend on the crystal length, so for a thin crystal this equation can be solved by analytically

$$C^{\ell,-\ell}_{p_i,p_s} \propto K^{|\ell|}_{p_i,p_s} \frac{\left(1-\gamma_i^2+\gamma_s^2\right)^{p_i}\left(1+\gamma_i^2-\gamma_s^2\right)^{p_s}\left(-2\gamma_i\gamma_s\right)^{|\ell|}}{\left(1+\gamma_i^2+\gamma_s^2\right)^{p_i+p_s+|\ell|}} \times {}_2F_1\left[\begin{matrix}-p_i,-p_s\\-p_i-p_s-|\ell|\end{matrix};\frac{1-\left(\gamma_i^2+\gamma_s^2\right)^2}{1-\left(\gamma_i^2-\gamma_s^2\right)^2}\right] \tag{3.8}$$

begin $\gamma_i = w_p/w_i$ idler and $\gamma_s = w_p/w_s$ signal are the ratios w_p/w_i and w_p/w_s [27]. The combinatorial coefficient and ${}_2F_1$ is the Gauss hypergeometric function. And the combinatorial coefficient $K^{|\ell|}_{p_i,p_s}$. Having a thick crystal, will not greatly affect the mode content of the SPDC state [27]. The simulation of the distribution (eq. (3.8)) for a Laguerre Gauss beam was carried out, it is presented in the figure 3.3.

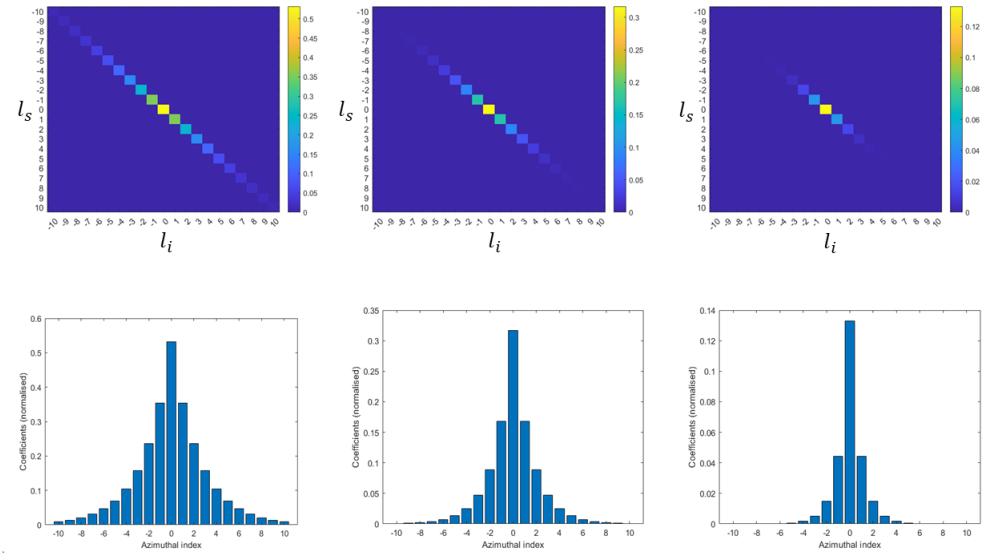

Figure 3.3: OAM distribution simulation. (a) measured coincidence counts, (b) only shows the diagonal elements of (a), which is commonly known as the measured spiral bandwidth.

4 Experimental Methods

An overview very simplified of the experiment is shown in Fig. 4.1 The experiment involves a two-photon source and a dedicated measurement branch for each photon. In this particular tests, the photons are obtained from SPDC within a BBO nonlinear crystal. The measurement process involves imaging the crystal onto Spatial Light Modulators (SLM) and subsequently onto single-mode fibers, which connect to individual single-photon detectors, that make a coincidence counting circuit. For the development and description of this experiment, inspiration was taken from the previous works of M. J. Padgett [4], M. J. Romero [8], and Carlos Sevilla [18].

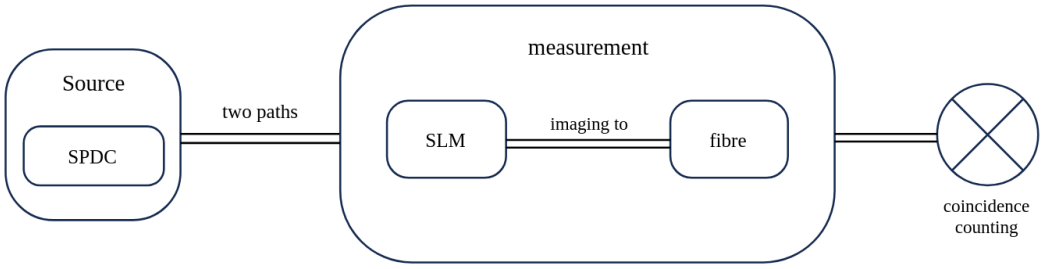

Figure 4.1: Overview experiment scheme.

4.1 Spatial Light Modulator

The experiments for studying the Orbital Angular Momentum entanglement were made using holograms [32, 35].

Looking for flexibility, the Spatial Light Modulator (SLM) was introduced. SLM is a voltage-controlled liquid crystal system 4.3. Changing the orientation of the liquid crystal results in changing the optical path difference of the input beam. This results in an individual phase profile in the reflected light [36]. Can be used to measure the spatial mode, OAM, and OAM superpositions. Also, the fact that the SLM holograms position can be adjusted by software, makes the alignment easier.

The applications of SLM are extensive, for generating complex functions, which is the case of this work [37, 38], and for producing complex 3D distributions of light [39, 40], in optical tweezers [41, 42],

4.2 Hologram generation

The SLM phase can take values from 0 to 2π as grayscale (0 to 255).

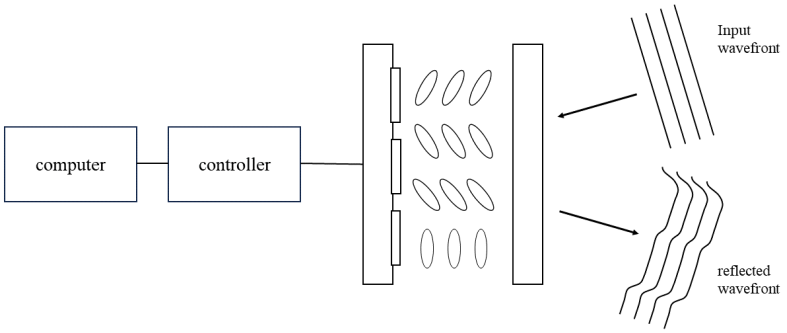

Figure 4.2: Diagram of the Spatial Light Modulator operation.

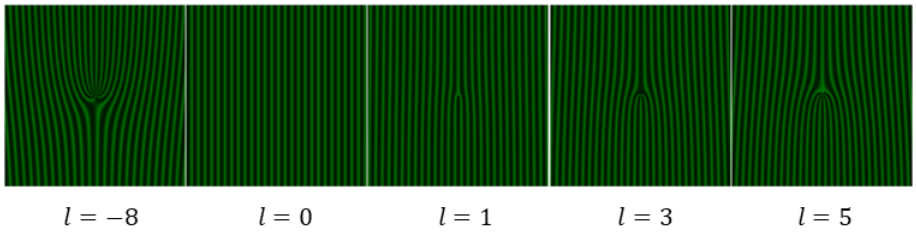

Figure 4.3: Examples of computer holograms for the LG p = 0 beams.

To encode hologram patterns like those shown in the figure 4.3, multiply the LG pattern from eq. (1.7) by linear phase grating with a d period,

$$M(x,y)e^{i[\phi(x,y)+2\pi x/d]} \tag{4.1}$$

The total phase is the sum of the LG phase term with the grating phase [43]. $M(x,y)$ is the amplitude and $\phi(x,y)$ the phase of the LG beam.

The relation between the phase and the grayscale is not completely linear. The characterization of this relation was previously made by C. A. Sevilla G. in his thesis work [18]. He used the same SLM, a HOLOEYE Pluto 1920×1800.

Their procedure to calibrate the SLM was the same used by Wei Han et al. [44], measuring the phase values in a complete period from $(0$ to $2\pi)$. The results are shown in fig. 4.4.

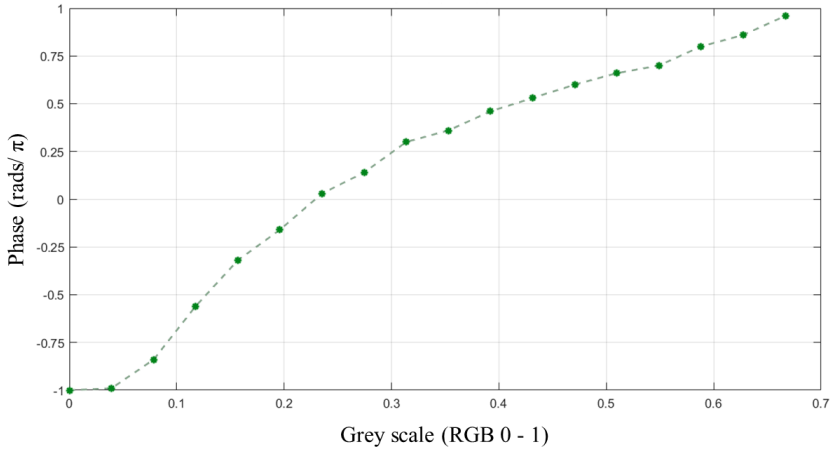

Figure 4.4: Phase vs. Grey Scale value un RGB (0 -1). Experimental obtain data, and the interpolation [18].

The experimental setup is shown in Figure 4.5. The laser source (Gaussian mode) is a MOGlabs laser with a wavelength of 405 nm past through a single mode fiber (SMF), resulting in a fundamental Gaussian beam. By a half-wave plate (HWP) the polarization is controlled in the axis of the crystal. Then the beam is focused, by a focal distance lens $L_2 = 1000$ mm, inside the BBO with dimensions $8 \times 8 \times 2$ mm^3. The wavelength of the laser pump is 405.2 nm, the emission angle is $3°$. The photons generated by the type-I collinear SPDC past for a bandpass filter (BPF) of $\Delta\lambda = 10$ nm around 808 nm to select the degenerate pair of photons.

4.3 Experimental setup

The pair of photons are separated by a beam splitter. With a knife edge mirror (KEM), both photons are directed to the SLM screen by mirrors with a $6°$ angle with an axis parallel to the SLM.

The SLM generated a Gaussian mode, that is re-imaged by two telescopes and arriving in single-mode fibers. These are conected to avalanche photodiodes for tallying incoming photons and calculating coincidence count rates.

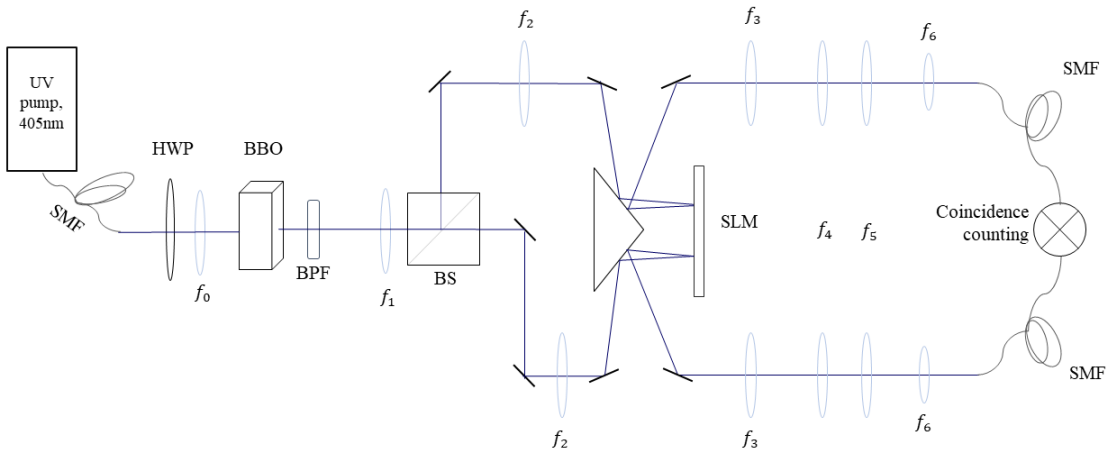

Figure 4.5: Experimental setup, $L_3 = 250$ mm, $L_4 = 100$ mm, $L_5 = 500$ mm, $L_6 = 8$ mm.

5 Quantum Entanglement

5.1 Einstein–Podolsky–Rosen paradox

The Einstein-Podolsky-Rosen (EPR) paradox, proposed in 1935, a thought experiment in quantum mechanics that challenges the principle of locality and highlights the phenomenon of entanglement [45]. According to the EPR paradox, when two particles are entangled, the measurement of a property of one particle instantaneously determines the corresponding property of the other, regardless of the distance between them. This seemingly implies faster-than-light communication, which contradicts the principle of locality in special relativity [45, 46, 47].

The paradox was developed by making two basic assumptions about nature, the locality, two sufficiently separate systems that do not interact with each other. And the reality, that refers to Einstein's theory of relativity [45, 8]. The fact is that if the state can be predicted, it has some physical reality, assuming that the condition is determined before measuring [48, 46].

5.2 Local hidden variable theory

The EPR paradox was reformulated in terms of spin (polarization) systems by David Bohm [49] (Fig. 5.1). Think about a entangled state specific [50, 51],

$$|\Psi_{s,i}\rangle = \frac{1}{\sqrt{2}}|H\rangle_A|H\rangle_B + |V\rangle_A|V\rangle_B \tag{5.1}$$

where V is the vertical polarization, H is the horizontal polarization, and the subscripts $\{A, B\}$ are the states of the signal and idle photons, also popularly called Alice and Bob photons, as an analogy to a pair of separate observers. These two photons are guided separately to their measuring station, with polarizer directions a and b. The polarizers are followed by detectors giving two possible results $+$ or $-$, determined by the polarization orientations [49, 48].

The probabilities P_{++}, P_{--}, P_{+-} and P_{-+} provide information about the results of the measurements. For example, if P_{++} and P_{--} are $1/2$ each, while P_{+-} and P_{-+} are 0. This suggests a surprising correlation: if the result on one photon is $+$, the result on the other photon will be $+$ with certainty (and the same for $-$). Although the individual measurements are random, there is a perfect correlation between the results of the entangled photons [45, 48].

One can then think of "additional parameters" that will determine the results, "hidden variables" (HV) [52].

5.2.1 Clauser, Horne, Shimony and Holt Bell-type inequalitie

John Bell published, in 1964, the derivation of a statistical limit of an inequality, Bell's inequality [53, 52]. There are some versions of this inecuality, Bell-type inequalities, one of them is the as proposed, in 1969, by Clauser, Horne, Shimony and Holt (CSHS) [54].

λ represent a the hidden variable, for a results of measurements, A and B, will deepens of λ and the orientations of the polarisers. Being $A(\lambda, \mathbf{a}) = \pm 1$ and $B(\lambda, \mathbf{b}) = \pm 1$. Can be expressed [53, 52, 55],

$$s = A(\lambda, \mathbf{a})B(\lambda, \mathbf{b}) - A(\lambda, \mathbf{a})B\left(\lambda, \mathbf{b}'\right) + A\left(\lambda, \mathbf{a}'\right)B(\lambda, \mathbf{b}) + A\left(\lambda, \mathbf{a}'\right)B\left(\lambda, \mathbf{b}'\right) \tag{5.2}$$

Since A and B can only be ± 1, with (5.2) $s = \pm 2$ For hidden variable probability distribution, $\rho(\lambda)$, the value of s is then, range from -2 to 2, then [8]

$$-2 \leq \int d\lambda \rho(\lambda) s\left(\lambda, \mathbf{a}, \mathbf{a}', \mathbf{b}, \mathbf{b}'\right) \leq 2 \tag{5.3}$$

Defining a correlation function E as,

$$E(\mathbf{a}, \mathbf{b}) = \int d\lambda \rho(\lambda) A(\lambda, \mathbf{a}) B(\lambda, \mathbf{b}) \tag{5.4}$$

and writing (5.2) in terms of (5.6), and (5.3),

$$-2 \leq E(\mathbf{a}, \mathbf{b}) - E\left(\mathbf{a}, \mathbf{b}'\right) + E\left(\mathbf{a}', \mathbf{b}\right) + E\left(\mathbf{a}', \mathbf{b}'\right) \leq 2 \tag{5.5}$$

The Bell parameter, S, defined as

$$S = E(\mathbf{a}, \mathbf{b}) - E\left(\mathbf{a}, \mathbf{b}'\right) + E\left(\mathbf{a}', \mathbf{b}\right) + E\left(\mathbf{a}', \mathbf{b}'\right) \tag{5.6}$$

S can take values up to $2\sqrt{2}$, this predicted by quantum mechanic.

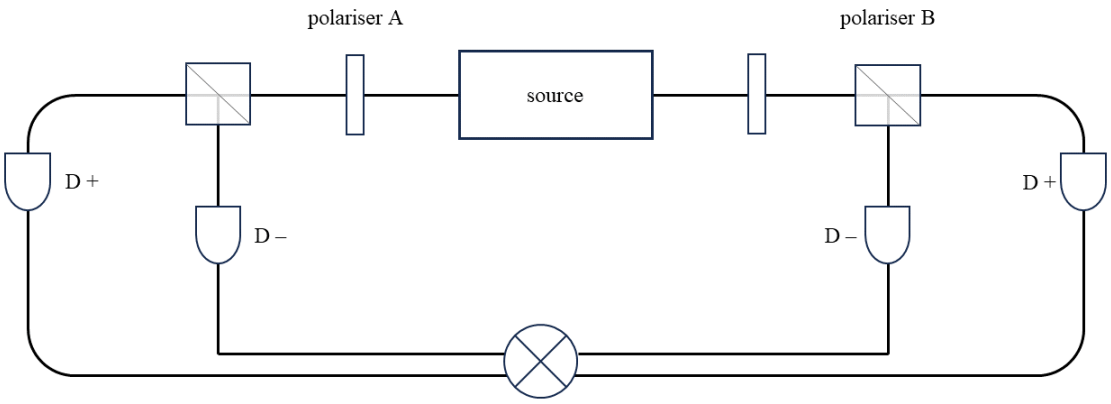

Figure 5.1: Aspect experiment [50], measure of the polarisation of photons.

Experimentally the correlation function, $E(\mathbf{a}, \mathbf{b})$ can be obtained from the coincidence count rate, $C_{\pm\pm}$ of the simultaneous detector measurements as[50]

$$E(\mathbf{a}, \mathbf{b}) = \frac{C_{++}(\mathbf{a}, \mathbf{b}) - C_{+-}(\mathbf{a}, \mathbf{b}) - C_{-+}(\mathbf{a}, \mathbf{b}) + C_{--}(\mathbf{a}, \mathbf{b})}{C_{++}(\mathbf{a}, \mathbf{b}) + C_{+-}(\mathbf{a}, \mathbf{b}) + C_{-+}(\mathbf{a}, \mathbf{b}) + C_{--}(\mathbf{a}, \mathbf{b})} \tag{5.7}$$

The results of the Aspect experiment 5.1 show that the coherence varies sinusoidally in direction between the two polarizers ($\Delta\theta$), and result in a value for S of 2.697 [50]. This demostrated to predict de observed correlations, local HV theories are no suffice.

.

6 Quantum Tests

6.1 Experimental results of the measured spiral bandwidth

Following the rigorous alignment procedure, the first test was to demonstrate the conservation of OAM. The measured of the spiral bandwidth shows in Figure 6.1, which is, experimentally, the coincidence counts.

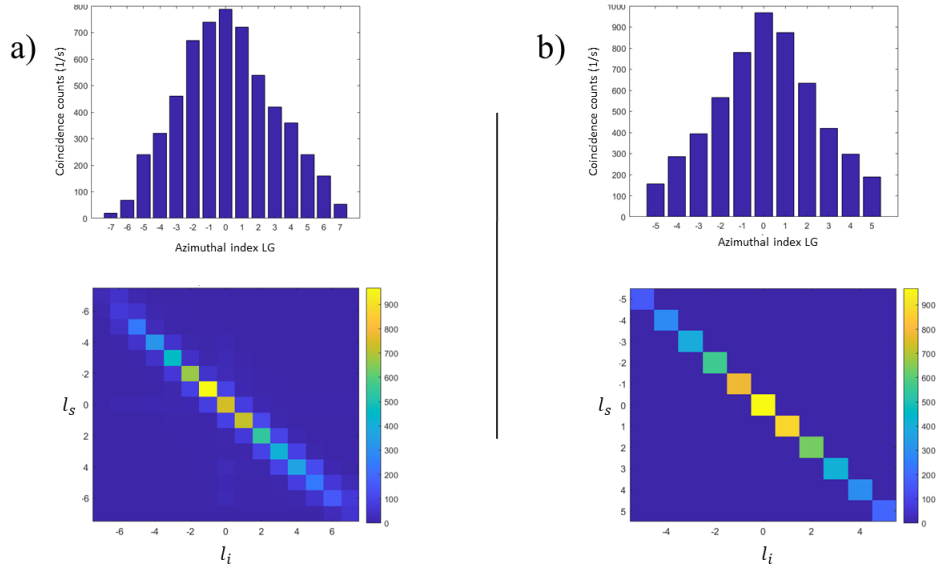

Figure 6.1: Experimental results, (a) and (b) show in a plot of the density of counts, and the spiral bandwidth. The FWHM of the SBW is approx. (a) 5, and (b) 4

Use of the experimental setup as shown Fig 6.1, each side of the SLM was programmed with holograms with the component ℓ from -7 to 7 (6.1 a)), and from -5 to 5. Note that the only SLM was split in two to create the branches.

In the experiment procedure, one of the sides changes the hologram projected constantly, while the other remains static, averaging 10 seconds of beads in coincidence for each combination.

Can be recognized The OAM conservation for the anti-correlated diagonal obtained.

There is also a decrease in the number of coincidences as the values of ℓ move away from zero. The Full Width Half Maximum (FWHM) in this case describes the width of a "bump" in the data. The values of the off-diagonal elements, theoretically, should be zero, but experimentally this is often not achievable because this measurements is very sensitive to misalignment.

Figure 6.1a shows the measurements taken before implementing an individual alignment of each of the 11 holograms within the SML display, thus obtaining the measurements in Figure 6.1b, where observe a clear improvement of the theoretically expected symmetry discussed in Section 4.5, Approximation for the SPDC mode funtion.

6.2 Analogy between polarization and OAM

For perfoming Bell's experiment using OAM, is expected to formulate an analogy between polarization and OAM.

Padgett and Courtial [56, 57] proposed a representation of the OAM states on a Bloch sphere equivalent to the Poincaré sphere, that represents the complex superposition.

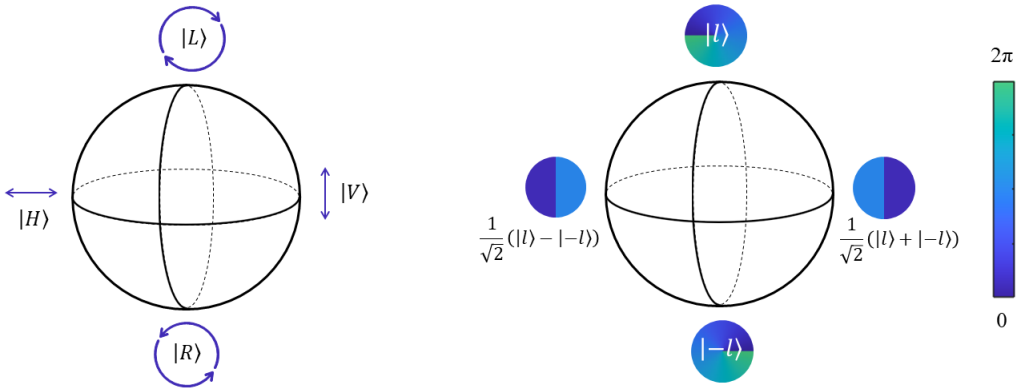

Figure 6.2: Bloch spheres (a) The superpositions of left- and right- circular polarisations (b) Analogous sphere for OAM, with the poles being $|\pm\ell\rangle$ [4].

For a given order, orthogonal OAM modes $|+\ell\rangle$ and $|-\ell\rangle$ can be placed in the north and the south poles on the Bloch sphere. A superposition of $|+\ell\rangle$ and $|-\ell\rangle$ with arbitrary relative phase is represented by a point along the equator (fig. 6.2) [4, 8],

$$|\theta\rangle = \frac{1}{\sqrt{2}}\left(e^{i\ell\theta}|+\ell\rangle + e^{-i\ell\theta}|-\ell\rangle\right) \tag{6.1}$$

6.2.1 Maximal bell inequality violation

To quantify the entanglement, it is necessary to show that the correlation between the pair of photons continues for superposition states. Using Eq. (6.1) and (3.5), the coincidence rate

$$C(\theta_A, \theta_B) = |\langle\theta_B|\langle\theta_A \mid \psi\rangle|^2 \propto= cos^2[l(\theta_A - \theta_B)] \tag{6.2}$$

The sinusoidal fringes of this joint probability are the signature of two-dimensional entanglement (see Eq. (6.1)) [4, 58, 59]

The angles that maximize the value of S described in the Eq. (5.6) can be obtained, using the following result of the procedure, and maximizing the function.

$$\begin{aligned} \langle\theta_A \mid \psi\rangle &= \left[e^{-i\theta_A}\left\langle + l\right|_A + e^{i\theta_A}\langle - l|_A\right]\left[\sum_l C_{l,-l}\left(|+l\rangle_A|-l\rangle_B + |-l_A|+l\rangle_B\right)\right] \\ &= C_{l,-}e^{-i\theta_A}|-l\rangle_B + C_{l,-l}e^{i\theta_A}|+l\rangle_B \end{aligned} \tag{6.3}$$

$$\begin{aligned} \langle\theta_B|\langle\theta_A \mid \psi\rangle &= \left[e^{-i\theta_B}\left\langle + l\right|_B + e^{+l\theta_B}\left\langle - l\right|_B\right]\left[C_{l,-l}\left(e^{-i\theta_A}|-l\rangle_B + e^{i\theta_A}|+l\rangle_B\right)\right] \\ &= C_{l,-l}\left[e^{i(\theta_A-\theta_B)} + e^{-i(\theta_A+\theta_B)}\right] \\ &= 2C_{l,-l}\cos\left(\theta_A - \theta_B\right) \end{aligned} \tag{6.4}$$

In this example case the inequality is maximally violated by the following values of the relative rotation angles between the holograms, $\theta_A = 0, \theta_B = \frac{\pi}{8\ell}, \theta'_A = \frac{\pi}{4\ell}$ and $\theta'_B = \frac{3\pi}{8\ell}$.

6.3 OAM Bell inequality

The same experimental setup was used to demonstrate the violation of Bell's inequality with OAM modes. In Sec. 3.2.1 It is mentioned that the Bloch sphere can be used to show an analogy between polarization and OAM.

analogously to the polarization tests, the holograms created for this part of the experiment are obtained from the expression REF, OAM superposition states, the degree of rotation being relative (see fig 6.3). The holograms used to measure the superposition states are described by:

$$|\psi\rangle = \frac{1}{\sqrt{2}}(|\ell\rangle + \exp(i\ell\theta)|-\ell\rangle)$$

For this case, the correlation function can be expressed as:

$$E\left(\theta_A,\theta_B\right)=\frac{C\left(\theta_A,\theta_B\right)+C\left(\theta_A+\frac{\pi}{2\ell},\theta_B+\frac{\pi}{2\ell}\right)-C\left(\theta_A+\frac{\pi}{2\ell},\theta_B\right)-C\left(\theta_A,\theta_B+\frac{\pi}{2\ell}\right)}{C\left(\theta_A,\theta_B\right)+C\left(\theta_A+\frac{\pi}{2\ell},\theta_B+\frac{\pi}{2\ell}\right)+C\left(\theta_A+\frac{\pi}{2\ell},\theta_B\right)+C\left(\theta_A,\theta_B+\frac{\pi}{2\ell}\right)}$$

where angles θ_A and θ_B are the angles on the different sides of the SLM obtained in the previous section. $C\left(\theta_A,\theta_B\right)$ is the coincidence count rate for each configuration of hologram orientations. Adapting Eq. (5.6) the S parameter can be written as

$$S\left(\theta_A,\theta_B\right)=E\left(\theta_A,\theta_B\right)-E\left(\theta_A,\theta'_B\right)+E\left(\theta'_A,\theta_B\right)-E\left(\theta'_A,\theta'_B\right)$$

For the OAM subspace $|\ell|$ determined, can be observed a violation of the inequality with a $S\leq 2$, confirming the observation of quantum correlations, and contradicting predictions by hidden variable theory.

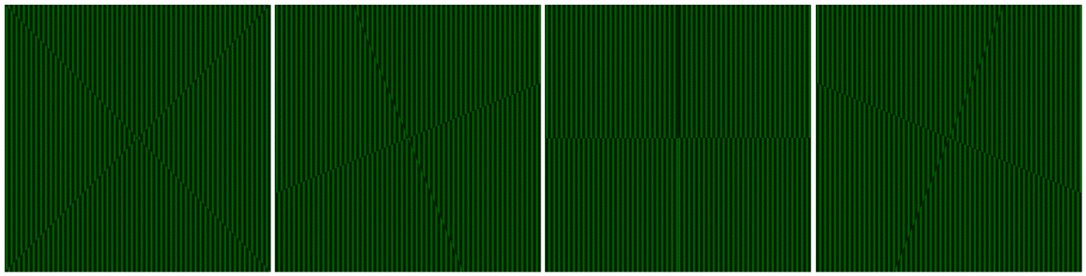

Figure 6.3: Holograms for LG superposition modes $\ell=2$, and rotations, $\theta_A=0,\theta_B=\frac{\pi}{8\ell},\theta'_A=\frac{\pi}{4\ell}$ and $\theta'_B=\frac{3\pi}{8\ell}$.

7 Conclusions and Perspectives

In this work, I have focused on the generation of type-I collinear SPDC two-photon states entangled in their orbital angular momentum (OAM) degree of freedom, when decomposed in the Laguerre-Gauss modes basis. We first discussed the Families of solutions of the paraxial wave equation before describing the angular momentum property attributed to photons of light beams carrying OAM and its process of generation and detection. This is an introduction to the understanding of photon correlation and entanglement in OAM.

Before moving on to the experimental methods used in this work, the basics of the SPDC process and its use as an entangled photon source are explained. The conservation of OAM and its correlation in both photos is described and justified theoretically, as well as analytically exposed with the approximation of the mode function in SPCD, which explains the spatial and spectral shape of the created photon modes. A simulation of the Spiral Bandwidth is made for comparison with experimental measurements.

The main objective of this work is the implementation and characterization of sources of interlaced photon quantum states in decomposed OAM in terms of the LaguerreGauss mode basis. The experimental setup is presented in the penultimate chapter.

As preliminary work, improvements to the experiment are discussed, such as the use of different crystals, like the PPKTP (Periodically Poled KTP) for a type II SPDC generation and a more efficient separation of the two generated photons. Or the use of two SLMs for better alignment. Data were taken to check the correlation of the OAM in the down-converted photons, as well as estimate the FWHM of the spiral bandwidth.

A detailed review of the view of quantum entanglement is given, starting with the Einstein-Podolsky Rosen (EPR) paradox, and concluding the section with an introduction to Bell-type inequalities.

In the last section, it exploited the analogy between a Poincare sphere and an OAM Bloch sphere to implement various tests of quantum mechanics. The procedure that was planned to be executed is described, and the experimental setup and the necessary knowledge were available, however, due to time and logistic issues, it was not possible to perform this last part in time. nevertheless, the presented is an introduction to future work on quantum information using optical resources.

A Appendix

A.1 Spiral Band Width (code)

```
% Parameters
gamma_i = 1.75;
gamma_s = 2.5;

l = -20:1:20;
f = gauss_hypergeometric__function(l, gamma_i, gamma_s);

% Function C(l)
C = ((-2 * gamma_i * gamma_s).^abs(l)) ./ ((1 + gamma_i^2 + gamma_s^2).^abs(l)).*f;

% Create the diagonal matrix with the diagonal values
SBW = diag(abs(C));

figure;
bar(l, abs(C));
xlabel('Azimuthal index LG');
ylabel('C(l)');
title('Coincidence count rate ');

plot(l, (abs(C)), 'b', 'LineWidth', 2);
grid on;
xlabel('Azimuthal index LG');
ylabel('C(l)');
title('OAM distribution');

figure;
imagesc(SBW);
colorbar;
xlabel('l_i');
ylabel('l_s');
title('ASpiral bandwidth');

figure;
bar(l, abs(C));
xlabel('Azimuthal index LG');
```

```
ylabel('C(l)');
title('OAM distribution');

% Hypergeometric Gauss function
function result = gauss_hypergeometric__function(l, gamma_i, gamma_s)
    z = (1 - (gamma_i^2 + gamma_s^2)^2)/(1 - (gamma_i^2 - gamma_s^2)^2);
    result = hypergeom(-l, [gamma_i, gamma_s], z);
end
```

References

[1] F.-G. Deng, B.-C. Ren, and X.-H. Li, "Quantum hyperentanglement and its applications in quantum information processing," 2017.

[2] T. P. Spiller, "Quantum information technology," *Materials Today*, vol. 6, no. 1, pp. 30–36, 2003. [Online]. Available: https://www.sciencedirect.com/science/article/pii/S1369702103001305

[3] J. Wang, F. Sciarrino, A. Laing, and M. G. Thompson, "Integrated photonic quantum technologies," *Nature Photonics*, vol. 14, no. 5, pp. 273–284, 2020. [Online]. Available: https://doi.org/10.1038/s41566-019-0532-1

[4] J. Leach, B. Jack, J. Romero, M. Ritsch-Marte, R. W. Boyd, A. K. Jha, S. M. Barnett, S. Franke-Arnold, and M. J. Padgett, "Violation of a bell inequality in two-dimensional orbital angular momentum state-spaces," *Optics Express*, vol. 17, no. 10, p. 8287, 2009. [Online]. Available: https://doi.org/10.1364/OE.17.008287

[5] D. J. Griffiths, "Resource letter em-1: Electromagnetic momentum," *American Journal of Physics*, vol. 80, no. 1, pp. 7–18, 2012. [Online]. Available: https://doi.org/10.1119/1.3641979

[6] B. Saleh and M. Teich, *Fundamentals of Photonics, 3rd Edition*. Wiley, 02 2019.

[7] A. E. Siegman, *Lasers*. Sausalito, CA: University Science Books, 1986.

[8] M. J. Romero, "Orbital angular momentum entanglement," Ph.D. dissertation, University of Glasgow, 2011.

[9] L.-P. Yang, F. Khosravi, and Z. Jacob, "Quantum field theory for spin operator of the photon," *Physical Review Research*, vol. 4, no. 2, p. 023165, 2022. [Online]. Available: https://doi.org/10.1103/PhysRevResearch.4.023165

[10] M. Genovese, "Research on hidden variable theories: A review of recent progresses," *Physics Reports*, vol. 413, no. 6, pp. 319–396, 2005. [Online]. Available: https://doi.org/10.1016/j.physrep.2005.03.003

[11] H. C. Ohanian, "What is spin?" *American Journal of Physics*, vol. 54, no. 6, pp. 500–505, 1986. [Online]. Available: https://doi.org/10.1119/1.14580

[12] C. G. Darwin, "Notes on the theory of radiation," *Proceedings of the Royal Society of London. Series A, Containing Papers of a Mathematical and Physical Character*, vol. 136, no. 829, pp. 36–52, 1932. [Online]. Available: https://doi.org/10.1098/rspa.1932.0065

[13] S. M. Barnett, M. Babiker, and M. J. Padgett, "Optical orbital angular momentum," *Philosophical Transactions of the Royal Society A: Mathematical, Physical and Engineering Sciences*, vol. 375, no. 2087, p. 20150444, 2017. [Online]. Available: https://doi.org/10.1098/rsta.2015.0444

[14] L. Allen, M. W. Beijersbergen, R. J. C. Spreeuw, and J. P. Woerdman, "Orbital angular momentum of light and the transformation of laguerre-gaussian laser modes," *Physical Review A*, vol. 45, no. 11, pp. 8185–8189, 1992. [Online]. Available: https://doi.org/10.1103/PhysRevA.45.8185

[15] M. Lax, W. H. Louisell, and W. B. McKnight, "From maxwell to paraxial wave optics," *Phys. Rev. A*, vol. 11, pp. 1365–1370, Apr 1975. [Online]. Available: https://link.aps.org/doi/10.1103/PhysRevA.11.1365

[16] V. Y. Bazhnenov, M. V. Vasnetsov, and M. S. Soskin, "Laser beams with screw dislocations in their wavefronts," *JETP Letters*, vol. 52, pp. 429–431, 1990.

[17] R. Chen, H. Zhou, M. Moretti, X. Wang, and J. Li, "Orbital angular momentum waves: Generation, detection, and emerging applications," *IEEE Communications Surveys & Tutorials*, vol. 22, no. 2, pp. 840–868, 2020. [Online]. Available: https://doi.org/10.1109/COMST.2019.2952453

[18] C. A. S. G., "Direct observation of conservation of oam in type-i collinear spdc," Ph.D. dissertation, Centro de Investigaciones en Óptica A.C., 2018.

[19] M. W. Beijersbergen, L. Allen, H. van der Veen, and J. P. Woerdman, "Astigmatic laser mode converters and transfer of orbital angular momentum," *Optics Communications*, vol. 96, pp. 123–132, 1993.

[20] R. Chen, H. Zhou, M. Moretti, X. Wang, and J. Li, "Orbital angular momentum waves: Generation, detection, and emerging applications," *IEEE Communications Surveys and Tutorials*, vol. 22, no. 2, pp. 840–868, 2020.

[21] D. A. Kleinman, "Theory of optical parametric noise," *Physical Review*, vol. 174, no. 3, pp. 1027–1041, 1968. [Online]. Available: https://doi.org/10.1103/PhysRev.174.1027

[22] S. Walborn, C. Monken, S. Pádua, and P. S. Ribeiro, "Spatial correlations in parametric down-conversion," *Physics Reports*, vol. 495, no. 4-5, pp. 87–139, oct 2010.

[23] C. Gerry and P. Knight, *Introductory Quantum Optics*. Cambridge University Press, 2005. [Online]. Available: https://books.google.com.mx/books?id=CgByyoBJJwgC

[24] F. M. Miatto, A. M. Yao, and S. M. Barnett, "Full characterization of the quantum spiral bandwidth of entangled biphotons," *Phys. Rev. A*, vol. 83, p. 033816, Mar 2011. [Online]. Available: https://link.aps.org/doi/10.1103/PhysRevA.83.033816

[25] D. C. Burnham and D. L. Weinberg, "Observation of simultaneity in parametric production of optical photon pairs," *Phys. Rev. Lett.*, vol. 25, pp. 84–87, Jul 1970. [Online]. Available: https://link.aps.org/doi/10.1103/PhysRevLett.25.84

[26] R. Boyd, *Nonlinear Optics*. Elsevier Science, 2003. [Online]. Available: https://books.google.com.mx/books?id=3vHb7WGXmSQC

[27] A. B. U'Ren, K. Banaszek, and I. A. Walmsley, "Photon engineering for quantum information processing," *Quantum Inf. Comput.*, vol. 3, pp. 480–502, 2003. [Online]. Available: https://api.semanticscholar.org/CorpusID:17791609

[28] C. Couteau, "Spontaneous parametric down-conversion," *Contemporary Physics*, vol. 59, no. 3, p. 291–304, Jul. 2018. [Online]. Available: http://dx.doi.org/10.1080/00107514.2018.1488463

[29] S. Feng and P. Kumar, "Spatial symmetry and conservation of orbital angular momentum in spontaneous parametric down-conversion," *Phys. Rev. Lett.*, vol. 101, p. 163602, Oct 2008.

[30] S. Franke-Arnold, S. M. Barnett, M. J. Padgett, and L. Allen, "Two-photon entanglement of orbital angular momentum states," *Phys. Rev. A*, vol. 65, p. 033823, Feb 2002. [Online]. Available: https://link.aps.org/doi/10.1103/PhysRevA.65.033823

[31] H. H. Arnaut and G. A. Barbosa, "Orbital and intrinsic angular momentum of single photons and entangled pairs of photons generated by parametric down-conversion," *Phys. Rev. Lett.*, vol. 85, pp. 286–289, Jul 2000.

[32] A. Mair, A. Vaziri, G. Weihs, and A. Zeilinger, "Entanglement of the orbital angular momentum states of photons," *Nature*, vol. 412, no. 6844, pp. 313–316, jul 2001. [Online]. Available: https://doi.org/10.1038%2F35085529

[33] M. Krenn, M. Malik, M. Erhard, and A. Zeilinger, "Orbital angular momentum of photons and the entanglement of laguerre–gaussian modes," *Philosophical Transactions of the Royal Society A: Mathematical, Physical and Engineering Sciences*, vol. 375, no. 2087, p. 20150442, Feb. 2017. [Online]. Available: http://dx.doi.org/10.1098/rsta.2015.0442

[34] J. P. Torres, A. Alexandrescu, and L. Torner, "Quantum spiral bandwidth of entangled two-photon states," *Physical Review A*, vol. 68, no. 5, p. 050301, 2003. [Online]. Available: https://doi.org/10.1103/PhysRevA.68.050301

[35] N. K. Langford, R. B. Dalton, M. D. Harvey, J. L. O'Brien, G. J. Pryde, A. Gilchrist, S. D. Bartlett, and A. G. White, "Measuring entangled qutrits and their use for quantum bit commitment," *Phys. Rev. Lett.*, vol. 93, p. 053601, Jul 2004.

[36] D. G. G. Jennifer E. Curtis, Brian A. Koss, "Dynamic holographic optical tweezers," *Optics Communications*, vol. 207, no. 1, pp. 169–175, 2002.

[37] R. S. Carl Paterson, "Higher-order bessel waves produced by axicon-type computer-generated holograms," *Optics Communications*, vol. 124, no. 1, pp. 121–130, 1996.

[38] J. Arlt, K. Dholakia, L. Allen, and M. Padgett, "The production of multiringed laguerre–gaussian modes by computer-generated holograms," *Journal of Modern Optics*, vol. 45, pp. 1231–1237, 06 1998.

[39] J. Leach, M. R. Dennis, J. Courtial, and M. J. Padgett, "Vortex knots in light," *New Journal of Physics*, vol. 7, no. 1, p. 55, feb 2005.

[40] J. Leach, G. Sinclair, P. Jordan, J. Courtial, M. J. Padgett, J. Cooper, and Z. J. Laczik, "3d manipulation of particles into crystal structures using holographic optical tweezers," *Opt. Express*, vol. 12, no. 1, pp. 220–226, Jan 2004.

[41] N. R. Heckenberg, R. McDuff, C. P. Smith, and A. G. White, "Generation of optical phase singularities by computer-generated holograms," *Opt. Lett.*, vol. 17, no. 3, pp. 221–223, Feb 1992.

[42] D. Grier, "A revolution in optical manipulation," *Nature*, vol. 424, pp. 810–6, 09 2003.

[43] J. B. Bentley, J. A. Davis, M. A. Bandres, and J. C. Gutiérrez-Vega, "Generation of helical ince-gaussian beams with a liquid-crystal display," *Opt. Lett.*, vol. 31, no. 5, pp. 649–651, Mar 2006.

[44] W. Han, Y. Yang, W. Cheng, and Q. Zhan, "Vectorial optical field generator for the creation of arbitrarily complex fields," *Opt. Express*, vol. 21, no. 18, pp. 20 692–20 706, Sep 2013.

[45] A. Einstein, B. Podolsky, and N. Rosen, "Can quantum-mechanical description of physical reality be considered complete?" *Phys. Rev.*, vol. 47, pp. 777–780, May 1935.

[46] M. D. Reid, "Demonstration of the einstein-podolsky-rosen paradox using nondegenerate parametric amplification," *Phys. Rev. A*, vol. 40, pp. 913–923, Jul 1989. [Online]. Available: https://link.aps.org/doi/10.1103/PhysRevA.40.913

[47] Z. Y. Ou, S. F. Pereira, H. J. Kimble, and K. C. Peng, "Realization of the einstein-podolsky-rosen paradox for continuous variables," *Phys. Rev. Lett.*, vol. 68, pp. 3663–3666, Jun 1992. [Online]. Available: https://link.aps.org/doi/10.1103/PhysRevLett.68.3663

[48] B. Jack, "Quantum entanglement of the spatial modes of light," Ph.D. dissertation, University of Glasgow, 2011.

[49] A. Aspect, P. Grangier, and G. Roger, "Experimental realization of einstein-podolsky-rosen-bohm gedankenexperiment: A new violation of bell's inequalities," *Phys. Rev. Lett.*, vol. 49, pp. 91–94, Jul 1982. [Online]. Available: https://link.aps.org/doi/10.1103/PhysRevLett.49.91

[50] A. Aspect, J. Dalibard, and G. Roger, "Experimental test of bell's inequalities using time-varying analyzers," *Phys. Rev. Lett.*, vol. 49, pp. 1804–1807, Dec 1982.

[51] A. Aspect, P. Grangier, and G. Roger, "Experimental tests of realistic local theories via bell's theorem," *Phys. Rev. Lett.*, vol. 47, pp. 460–463, Aug 1981.

[52] J. S. Bell, "On the problem of hidden variables in quantum mechanics," *Rev. Mod. Phys.*, vol. 38, pp. 447–452, Jul 1966.

[53] ——, "On the einstein podolsky rosen paradox," *Physics Physique Fizika*, vol. 1, pp. 195–200, Nov 1964. [Online]. Available: https://link.aps.org/doi/10.1103/PhysicsPhysiqueFizika.1.195

[54] J. F. Clauser, M. A. Horne, A. Shimony, and R. A. Holt, "Proposed experiment to test local hidden-variable theories," *Phys. Rev. Lett.*, vol. 23, pp. 880–884, Oct 1969.

[55] J. Bell, *Speakable and Unspeakable in Quantum Mechanics: Collected Papers on Quantum Philosophy*, ser. Collected papers on quantum philosophy. Cambridge University Press, 2004. [Online]. Available: https://books.google.com.mx/books?id=FGnnHxh2YtQC

[56] L. Allen, J. Courtial, and M. J. Padgett, "Matrix formulation for the propagation of light beams with orbital and spin angular momenta," *Phys. Rev. E*, vol. 60, pp. 7497–7503, Dec 1999.

[57] M. J. Padgett and J. Courtial, "Poincaré-sphere equivalent for light beams containing orbital angular momentum," *Opt. Lett.*, vol. 24, no. 7, pp. 430–432, Apr 1999.

[58] P. G. Kwiat, A. M. Steinberg, and R. Y. Chiao, "High-visibility interference in a bell-inequality experiment for energy and time," *Phys. Rev. A*, vol. 47, pp. R2472–R2475, Apr 1993. [Online]. Available: https://link.aps.org/doi/10.1103/PhysRevA.47.R2472

[59] C. Jebarathinam, J.-C. Hung, S.-L. Chen, and Y.-C. Liang, "Maximal violation of a broad class of bell inequalities and its implication on self-testing," *Phys. Rev. Res.*, vol. 1, p. 033073, Nov 2019.